atmosphere

MDPI

Article

Characterizing Dust and Biomass Burning Events from Sentinel-2 Imagery

Simone Lolli [1,*,†], Luciano Alparone [2], Alberto Arienzo [1,2] and Andrea Garzelli [3]

[1] CNR-IMAA, Consiglio Nazionale delle Ricerche, 85050 Potenza, Italy; alberto.arienzo@unifi.it
[2] Department of Information Engineering, University of Florence, 50139 Florence, Italy; luciano.alparone@unifi.it
[3] Department of Information Engineering and Mathematics, University of Siena, 53100 Siena, Italy; andrea.garzelli@unisi.it
* Correspondence: simone.lolli@cnr.it
† Current address: Contrada S. Loja snc, Tito Scalo, 85050 Potenza, Italy.

Abstract: The detection and evaluation of biomass burning and dust events are critical for understanding their impact on air quality, climate, and human health, particularly in the Mediterranean region. This research pioneers an innovative methodology that uses Sentinel-2 multispectral (MS) imagery to meticulously pinpoint and analyze long-transport dust outbreaks and biomass burning phenomena, originating both locally and transported from remote areas. We developed the dust/biomass burning (DBB) composite normalized differential index, a tool that identifies clear, dusty, and biomass burning scenarios in the selected region. The DBB index jointly employs specific Sentinel-2 bands: B2-B3-B4 for visible light analysis, and B11 and B12 for short-wave infrared (SWIR), exploiting the specificity of each wavelength to assess the presence of different aerosols. A key feature of the DBB index is its normalization by the surface reflectance of the scene, which ensures independence from the underlying texture, such as streets and buildings, for urban areas. The differentiation involves the comparison of the top-of-atmosphere (TOA) reflectance values from aerosol events with those from clear-sky reference images, thereby constituting a sort of calibration. The index is tailored for urban settings, where Sentinel-2 imagery provides a decametric spatial resolution and revisit time of 5 days. The average values of DBB achieve a 96% match with the coarse-mode aerosol optical depths (AOD), measured by a local station of the AERONET network of sun-photometers. In future studies, the map of DBB could be integrated with that achieved from Sentinel-3 images, which offer similar spectral bands, albeit with much less fine spatial resolution, yet benefit from daily coverage.

Keywords: AERONET; aerosols; atmospheric scattering; Sentinel-2

Citation: Lolli, S.; Alparone, L.; Arienzo, A.; Garzelli, A. Characterizing Dust and Biomass Burning Events from Sentinel-2 Imagery. *Atmosphere* **2024**, *15*, 672. https://doi.org/10.3390/atmos15060672

Academic Editor: Avelino Eduardo Saez

Received: 30 March 2024
Revised: 22 May 2024
Accepted: 28 May 2024
Published: 31 May 2024

1. Introduction

Aerosols are tiny short-lived particles suspended in the atmosphere that can originate from natural sources or human activities. Their various features and impacts have attracted considerable attention in many scientific disciplines. Recent studies, exemplified in [1], emphasize the crucial importance of the chemical composition of atmospheric aerosols in the influence of both health and climate. This influence occurs through processes such as light scattering and absorption (direct impact), as well as alteration of cloud properties (indirect impact) and air quality in the boundary layer [2]. Another study [3] explores the intricate impact of aerosols on precipitation behaviors, demonstrating their ability to increase or inhibit rainfall, which depends on their levels and functions as nuclei of cloud condensation. Aerosols also play an important role in the field of solar energy by influencing the interaction with solar radiation [4]. Their presence in the atmosphere can affect the efficiency of solar panels by scattering and absorbing solar radiation, which can reduce the amount of sunlight reaching the solar cells [5].

Among all different aerosol species, the detection of biomass burning events [6] and dust outbreaks using multispectral (MS) imagery, particularly in the Mediterranean region, represents a critical area of remote sensing research, as these events are increasingly influencing air quality. The unique geographic and climatic characteristics of the Mediterranean make it susceptible to frequent dust events from the Sahara [7] and biomass burning advections, both of which have significant implications for air quality, climate, and human health. Furthermore, the Mediterranean region is defined as a "climate hotspot", where climate change occurs more rapidly than in other parts of the world [8,9]. During the last decade, the Sentinel satellites, which are a component of the Copernicus program of the European Space Agency (ESA), have become crucial for observing these occurrences because of their sophisticated MS imaging capabilities.

The burning of biomass, such as wildfires and agricultural fires, primarily due to the clearing of land by land owners [10], injects substantial amounts of aerosols and trace gases into the atmosphere, affecting both air quality and climate. Sentinel-2, with its high-resolution MS imager, has been instrumental in detecting and monitoring these events. The combination of Sentinel-2's visible, near infrared (NIR), and short-wave infrared (SWIR) bands enables the differentiation of burned areas from their surroundings, exploiting the distinct reflectance properties of burned vegetation and soil. For example, in [11] the authors highlighted the potential of using the Sentinel-2 multi-wavelength sensor to directly detect severe aerosols burning biomass by incorporating polarization data, significantly improving detection accuracy [11]. Furthermore, algorithms developed for Sentinel-2 data have advanced the identification and mapping of burned areas, allowing near-real-time monitoring of biomass burning events. Techniques that use machine learning and deep learning approaches have shown promising results in improving the accuracy and efficiency of the detection and classification of burned areas, as demonstrated in a recent study [12].

Shifting the focus to another major atmospheric issue, dust, primarily from the Sahara, poses a distinct challenge in aerosol monitoring. It significantly impacts air quality, sunlight exposure, and ecosystems [7,13,14]. Sentinel-3, equipped with the Ocean and Land Color Instrument (OLCI) and the Sea and Land Surface Temperature Radiometer (SLSTR), provides important information for identifying and monitoring dust events. Sentinel-3's MS capabilities allow the identification of dust plumes through specific band combinations and indices, such as the Dust Index or the Normalized Difference Dust Index (NDDI), which take advantage of the distinct spectral signatures of dust in the atmosphere [15]. However, the spatial resolution of Sentinel-3 is insufficient for studies in urban settings.

Additional research incorporates a combination of various remote sensing methods: data from operational lidar and sun-photometer networks together with Sentinel data are used to study Saharan dust and biomass burning aerosols during the post-hurricane Ophelia, demonstrating the synergistic benefits of satellite and terrestrial observations in tracking aerosols [16]. Similarly, ref. [17] shows that the combined use of ceilometers, sun-photometers, and MS images effectively identifies events of burning of dust and biomass. Moreover, lidar technology alone is capable of differentiating various types of aerosols in an urban environment [18]. Despite these advances, challenges remain [19], particularly in urban settings where high spatial resolution is essential for street-level detection.

In Table 1, the different MS satellite instruments used during the last two decades to retrieve AOD are summarized, with their main technical characteristics. The primary MS sensors used to retrieve the optical depth of the aerosol and detect dust outbreaks differ in terms of spatial resolution, revisit time, and spectral coverage. MODIS offers moderate spatial resolution (250 m to 1 km) with daily revisit times, covering a wide spectral range that extends up to 14,385 nm, enabling comprehensive atmospheric studies. MISR, with a spatial resolution of 275 m–1.1 km, revisits every 9 days and focuses on narrow bandwidths in (443, 866) nm. VIIRS, onboard three satellites, provides a less than daily revisit time, with spatial resolution (375–750 m) comparable to MODIS, spanning a spectral range of 412 nm to 12,000 nm, allowing for detailed aerosol detection. OMI, though limited in spatial

resolution at 13 km × 24 km, offers daily revisits and focuses on ultraviolet-to-visible light ranges (264 nm to 504 nm), ideal for atmospheric trace gas analysis.

Table 1. Comparison of MS sensors with orbit characteristics. SS = sun-synchronous near-polar orbit.

Sensor(s)/Platform(s)	Spatial Resolution	Revisit Time	Spectral Coverage	Orbit	Refs.
MODIS/Terra & Aqua	250 m/500 m/1 km	Daily	405–14,385 nm	SS at ~705 km	[20]
MISR/Terra	275 m–1.1 km	9 days	443–866 nm	SS at ~705 km	[21]
VIIRS/Suomi NPP & NOAA 20 & 21	375–750 m	14 h	412–12,000 nm	SS at ~830 km	[20,22]
OMI/Aura	13 km × 24 km	Daily	264–504 nm	SS at ~705 km	[23]
MSI/Sentinel-2 A & B	10 m/20 m/60 m	5 days	429–2280 nm	SS at ~786 km	[22]
OLCI & SLSTR/Sentinel-3 A & B	300 m/500 m/1 km	Daily	400–12,000 nm	SS at ~814 km	[22]
TROPOMI/Sentinel-5P	7 km × 7 km	Daily	270–2380 nm	SS at ~824 km	[24]
OLI & OLI 2/LandSat 8 & 9	15 m/30 m/100 m	16 days	400–12,500 nm	SS at ~705 km	[20]
AIRS/Aqua	13.5 km	Daily	3700–15,400 nm	SS at ~705 km	[24]

Sentinel-2 constitutes a pivotal Earth observation (EO) project within the Copernicus program of ESA [25]. It incorporates two polar orbiting satellites, Sentinel-2A and Sentinel-2B [26]. Each satellite is equipped with an MS instrument (MSI) that captures 13 spectral bands almost embracing the solar spectrum over a 290 km orbital swath. The frequency of revisit is reduced to 5 days when both satellites are in formation. Thanks to their decametric spatial resolution, Sentinel-2 MS images have been used in forest surveillance [27], assessment of changes in land cover [28], and management of natural disasters [29]. In recent years, Sentinel-2 imagery has also played a key role in atmospheric studies, assessing both qualitative and quantitative analysis of aerosol and cloud optical properties. Sentinel-2 stands out for its high spatial resolution and revisit time, making it valuable for detailed monitoring of aerosols and surface phenomena at urban scales. Its spectral coverage (429 nm to 2280 nm) allows advanced vegetation and atmospheric studies to be accomplished, and surpasses many other sensors in terms of versatility and spatial detail. The twin satellites are providing valuable information on the optical properties of atmospheric constituents which are crucial to understanding air quality [30]. MS images also help study the characteristics of clouds, supporting the evaluation of their optical properties and radiative effects, which are essential for climate modeling [31].

Sentinel-3 complements Sentinel-2 with moderate resolution (300 m for the visible-NIR (V-NIR) OLCI instrument, 500 m and 1 km for the SLSTR instrument in the V-NIR/SWIR and thermal IR (TIR), respectively) but a broader spectral range (400–12,000 nm) for comprehensive ocean and land monitoring. Sentinel-5P focuses on atmospheric composition, offering daily revisits at a spatial resolution of 7 km × 7 km with a spectral range in 270–2380 nm. The Landsat family, with its extensive archive of 30 m Thematic Mapper (TM) and Operational Land Imager (OLI) images, offers a unique historical series for EO. Lastly, AIRS, with its bands embracing the emissive spectrum, excels in profiling atmospheric temperature and humidity, offering insights into weather patterns and climate. Unique in this list, it is capable of working with cloudy covers and even nighttime acquisitions.

2. Materials and Methods

2.1. Sentinel-2 Image Products and Formats

The Sentinel-2 twin satellite constellation (Sentinel-2 A/B), provides MS image data in the V-NIR and SWIR wavelengths, providing global Earth coverage with a 5-day revisit period [32]. Among the 13 bands of Sentinel-2 A/B, whose layout is shown in Figure 1, the VNIR bands, specifically B2, B3, B4, and B8, have the highest spatial resolution and a ground sampling distance of 10 m (GSD). B5, B6, and B7, in the red edge (RE) region, B11 and B12, in the SWIR region, and B8a, a narrowband near-infrared (NIR) centered at 865 nm, are provided at an intermediate resolution of 20 m GSD. The three lower-resolution bands available at 60 m GSD, B1, B9, and B10, are less relevant for EO and are used mainly for atmospheric studies, to recover the content of coastal aerosols, water vapor,

and cloud ice, respectively. The difference in spatial resolutions is a consequence of the fundamental trade-off in the design of electro-optical systems between spatial resolution, spectral resolution, and radiometric sensitivity [33]. Enhancing the resolution of MS data sets is generally performed thanks to the availability of a panchromatic image, using multiresolution analysis [34].

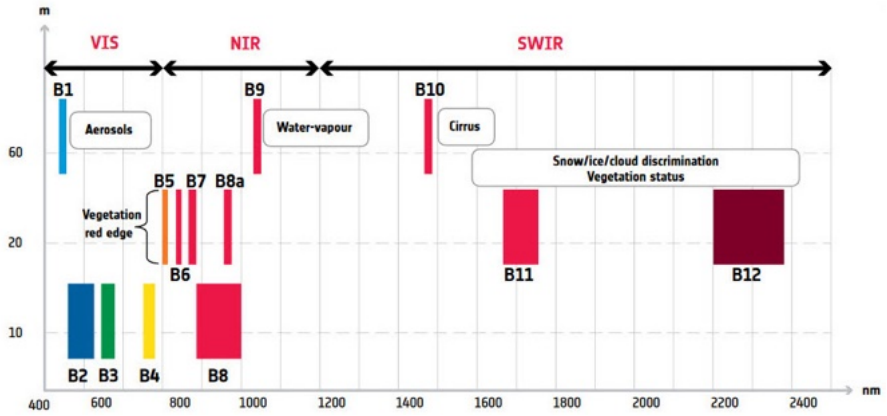

Figure 1. Sentinel-2 layout of spectral bands. Each band targets specific features: B1 for aerosols, B5 to B7 and B8a for vegetation including the red edge, B6, and B8 for broad vegetation analysis, B9 for water vapor, B10 for cirrus clouds, and B11 and B12 for snow/ice/cloud discrimination and advanced vegetation status monitoring. The wavelengths range from 400 nm to 2400 nm, with band widths indicated by the length of colored bars against a scale in meters (m) on the vertical axis.

Remote sensing optical data are available in spectral radiance (radiance normalized to the width of the spectral interval of the instrument) and reflectance formats. The reflectance, which is implicitly spectral, ranges in [0, 1] and can be defined as top-of-atmosphere (TOA) reflectance or as surface reflectance [35]. The former is the surface spectrum as viewed through the atmosphere by the satellite; it is given by the TOA spectral radiance rescaled by the TOA spectral irradiance of the Sun. The latter represents the spectral signature of the imaged surface; its determination requires the estimation, by parametric modeling and/or measurements, of the upward and downward transmission coefficients of the atmosphere and of the upward scattered radiance at TOA, a.k.a., the path radiance [36]. In addition to TOA spectral radiance, which is a level-one product (L1), the TOA reflectance, the L1C product, is generally available for systems featuring a nadir acquisition and global Earth coverage, such as Landsat 7 Enhanced Thematic Mapper Plus (ETM+), LandSat 8-9 Operational Land Imager (OLI), and Sentinel-2 A/B [37]. Surface reflectance is a level-two product (L2A) and is also distributed for global coverage systems. Sentinel-2 L1C and L2A products are available free online from ESA.

2.2. AERONET

AERONET, which stands for Aerosol Robotic Network [38], consists of a network of homogeneous ground-based sun photometers, deployed around the world, established by the National Aeronautics and Space Administration (NASA) Earth Observation Program. Each permanent and temporal observation site is managed by academic institutions and government organizations. Sun photometers, manufactured by Cimel Electronique, have played a crucial role in evaluating the properties of aerosols and clouds, largely because of the reliable and enduring measurements provided by AERONET. Such data are crucial for synergy with satellite data and for improving the understanding of how aerosols affect the environment and climate. The AERONET database, freely available at https://aeronet.gsfc.nasa.gov/ (accessed on 30 April 2024), is open to the public and is widely used by researchers, government organizations, and various stakeholders around the world to inform policy development and improve scientific understanding of the Earth system. Network efficiency comes primarily from the consistency of the tools, measurement

protocols, and data analysis methods used. This ensures that the data and analysis are reliable and consistent.

AERONET utilizes ground-based sun photometers to spectrally measure the aerosol optical depth (AOD) at different wavelengths, allowing for the derivation of fine- and coarse-mode optical depths at a reference wavelength of 500 nm through the aerosol spectral deconvolution algorithm (SDA). This method distinguishes between the optical depth of the cloud as the coarse-mode component and the fine-mode AOD [39], even under mixed cloud-aerosol conditions, allowing analysis of the influence of clouds on fine-mode AOD enhancements. Studies using AERONET data have revealed significant seasonal and regional variations in fine-mode AOD enhancements due to factors such as hygroscopic growth of particles and in-cloud processing, with notable differences observed across different global regions, including East Asia, North America, and Europe [40].

Further research has focused on the characterization of the aerosol size properties and their impact on AOD recovery, highlighting the importance of considering both fine and coarse aerosol modes to understand the aerosol dynamics and their climatic implications [41]. We use the products of version 3 level 1.5 [42]. Fine- and coarse-mode aerosol products are essential to evaluate the existence of burning of dust and/or biomass in a specific area. The retrieval method performs a spectral breakdown of the AOD data to distinguish between the impacts of fine particles (usually smaller and associated with human activities or secondary natural aerosols) and coarse particles (typically larger and originating from primary natural sources such as dust and sea salt). This differentiation is essential to characterize the type of aerosol present in a specific location.

2.3. Datasets

We have identified three test locations to collect Sentinel-2 L1C and L2A data, with simultaneous availability of aerosol data from an AERONET ground station. A 148 km^2 area near the city of Potenza, Italy, was selected as the first test site that included the AERONET sun photometer located at 40.60 ° N, 15.72 ° E, and 770 m elevation. Sentinel-2 L1C and L2A images—with the lower-resolution bands bicubically resampled at 10 m GSD—acquired on 6 June 2021, have been collected as a clear-sky reference (AOD < 0.07 measured by the AERONET ground station). Note that a single clear-sky reference date is required to calculate the spectral index for aerosol characterization, as described in Section 2.4.2. A 90-km^2 portion of the scene is shown in Figure 2, using two color compositions of the surface reflectance of the reference acquisition, i.e., true color (B4-B3-B2) and false color (B12-B11-B1). Two other L1C acquisitions over the same area have been downloaded for testing: one taken on 26 July 2020, to prove the capability of recognizing low aerosol depth, and the other taken on 10 August 2021 as an example of a moderate Saharan dust aerosol event. The true and false color compositions are shown in Figures 3 and 4.

A second test site has been considered in a Barcelona metropolitan area, Spain, where an AERONET station is present at 41.39 ° N, 2.11 ° E and 125 m elevation. We have collected Sentinel-2 images on a 243 km^2 region that includes urban, vegetated, and sea areas. The clear sky reference acquisition (Figure 5) was taken on 22 May 2020. The other three L1Ca 41.39 ° N, 2.11 °. The same area has been downloaded for testing: the first was taken on 27 May 2020 to prove the capability of recognizing low aerosol depth, the second was taken on 21 July 2021 as an example of a Saharan dust aerosol event, and the third acquisition was made on 25 October 2020 corresponding to a biomass burning event. The compositions of the true and false colors in the same 90 km^2 detail are shown in Figures 6 and 7.

The third testing location covers a region of 547 km^2 on the northern side of Tenerife Island (Spain) where an AERONET station is present at 28.47 ° N, 16.25 ° W, and 52 m elevation. The site was selected as a calibration test in the presence of a severe Saharan dust storm that occurred on 30 January 2022. Similarly to the other test sites, Figure 8 shows the surface reflectance of the reference clear-sky acquisition taken on 1 January 2020, while Figures 9 and 10 illustrate the true and false color compositions of the TOA reflectance, for a low-AOD acquisition on 14 February 2021 and the dust event on 30 January 2022.

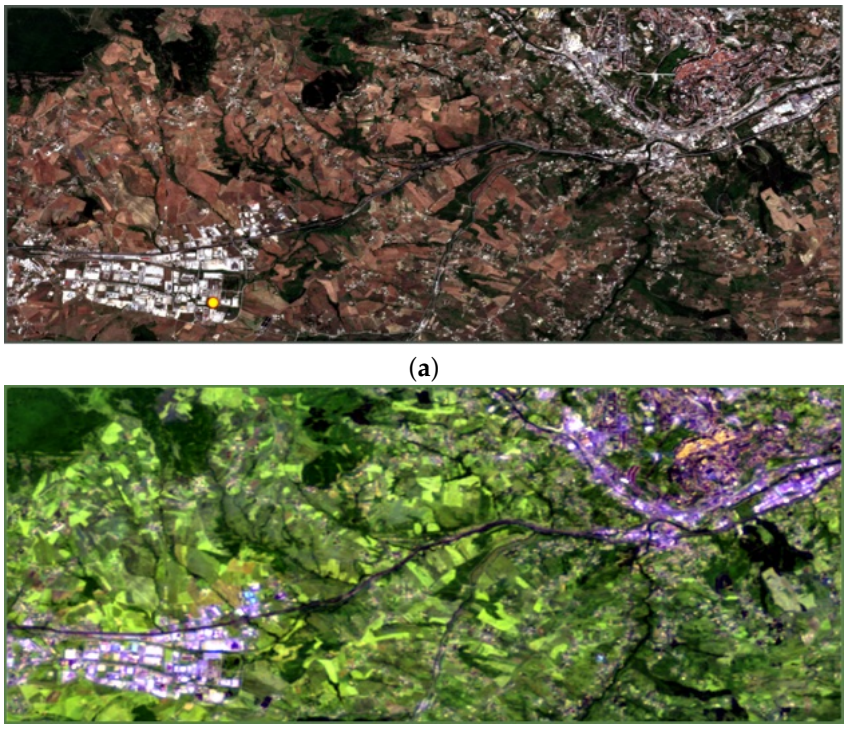

(**a**)

(**b**)

Figure 2. Some 90 km^2 portions of B4-B3-B2 (**a**) and B12-B11-B1 (**b**) color compositions of Sentinel-2 surface reflectance of the 6 July 2021 Potenza reference acquisition. The yellow circle in (**a**) indicates the AERONET instrument position.

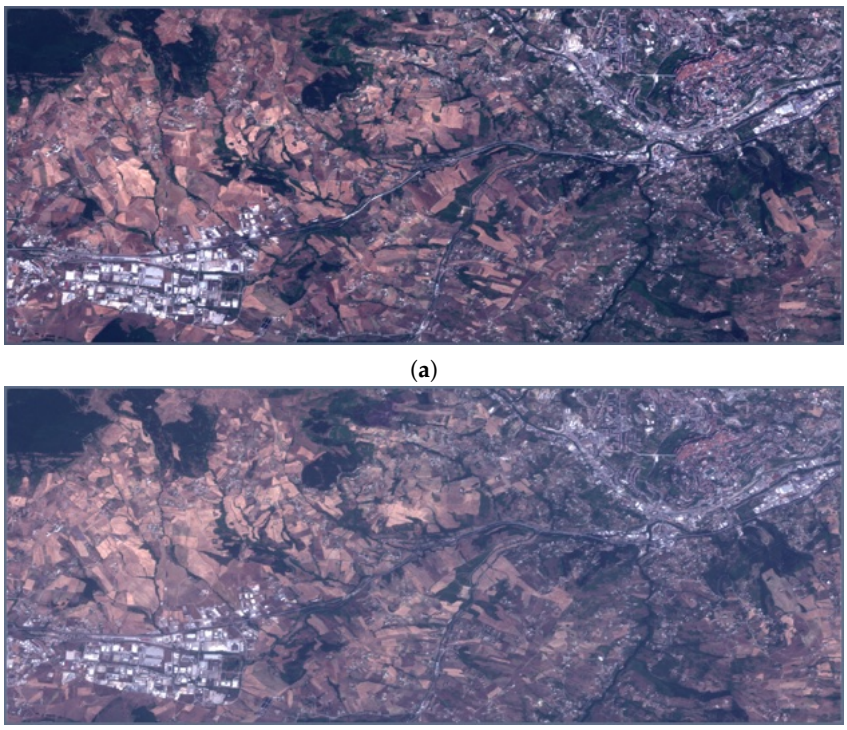

(**a**)

(**b**)

Figure 3. Some 90 km^2 portions of Potenza Sentinel-2 TOA reflectance B4-B3-B2 color compositions: (**a**) clear sky, 26 July 2020; (**b**) dust event, 10 August 2021.

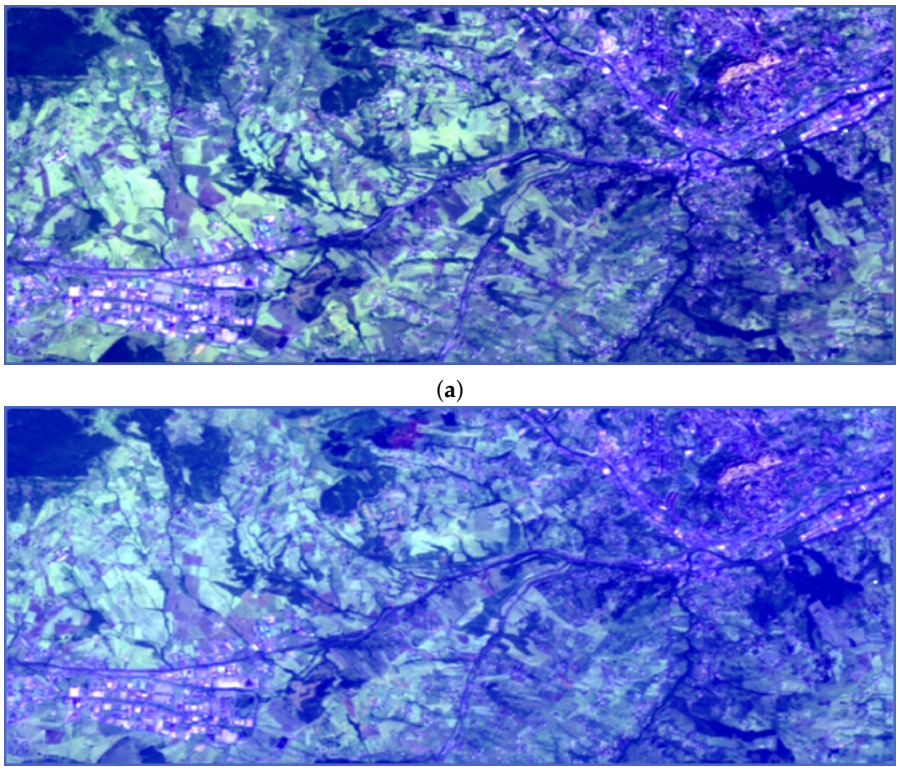

(**a**)

(**b**)

Figure 4. Some 90 km^2 portions of Potenza Sentinel-2 TOA reflectance B12-B11-B1 color compositions: (**a**) clear sky, 26 July 2020; (**b**) dust event, 10 August 2021.

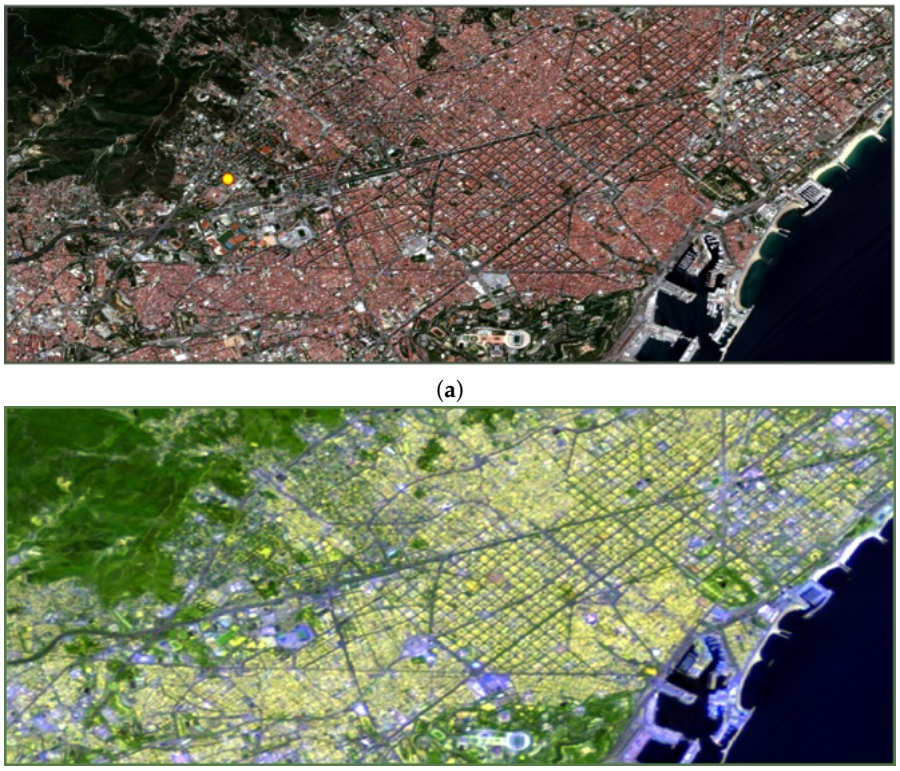

(**a**)

(**b**)

Figure 5. Some 90 km^2 portions of B4-B3-B2 (**a**) and B12-B11-B1 (**b**) color compositions of Sentinel-2 surface reflectance of the 22 May 2020 Barcelona reference acquisition. The yellow circle in (**a**) indicates the AERONET instrument position.

2.4. Aerosol Characterization

2.4.1. Selection of Sentinel-2 Bands

Upon visual examination of L1C images under varying aerosol types and conditions, it is evident that focusing on specific Sentinel-2 bands is crucial for aerosol characterization, particularly for distinguishing low AODs, dust aerosol conditions, and biomass burning events. The coastal (violet) band B1 is moderately useful for detecting dust aerosols, but not combustion aerosols, being dominated by Rayleigh scattering. The three visible bands (B2-B3- B4) are fully adequate for both types of aerosols. The SWIR bands, B11 at 1600 nm and especially B12 at 2200 nm, stand out as particularly advantageous for discriminating dust aerosols from biomass burning. Figures 6 and 7 for the Barcelona site show a departure from clear sky conditions in divergent directions during dust and biomass burning events. Figures 3 and 4 further support this notion during moderate dust aerosol conditions over Potenza, while Figures 9 and 10 corroborate it during an extreme dust event over Tenerife. These visual observations underscore the importance of using specific Sentinel-2 bands for accurate aerosol characterization under different environmental conditions.

(**a**)

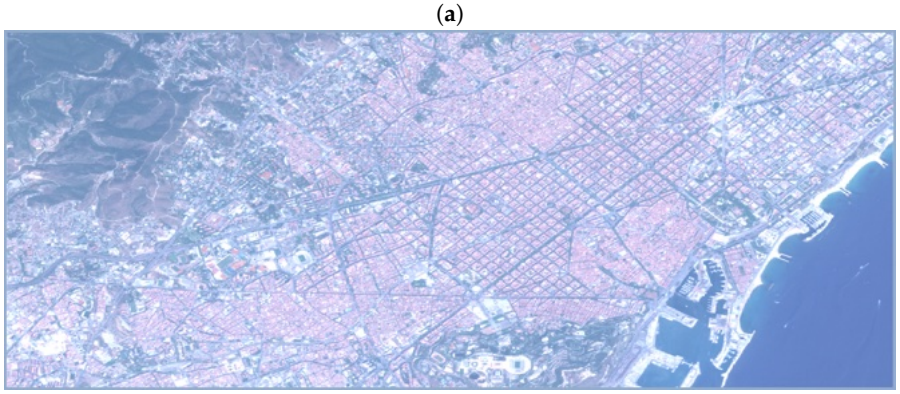

(**b**)

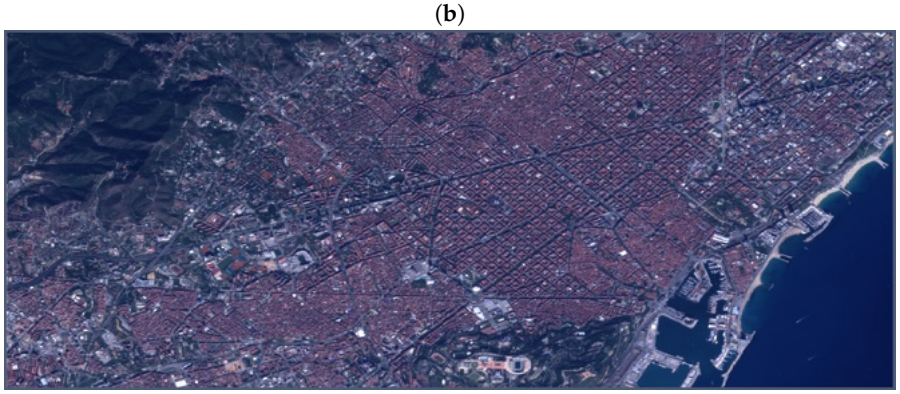

(**c**)

Figure 6. Some 90 km^2 portions of Barcelona Sentinel-2 TOA reflectance B4-B3-B2 color compositions: (**a**), clear sky, 27 May 2020; (**b**), dust event, 21 July 2022; (**c**), biomass burning event, 25 October 2020.

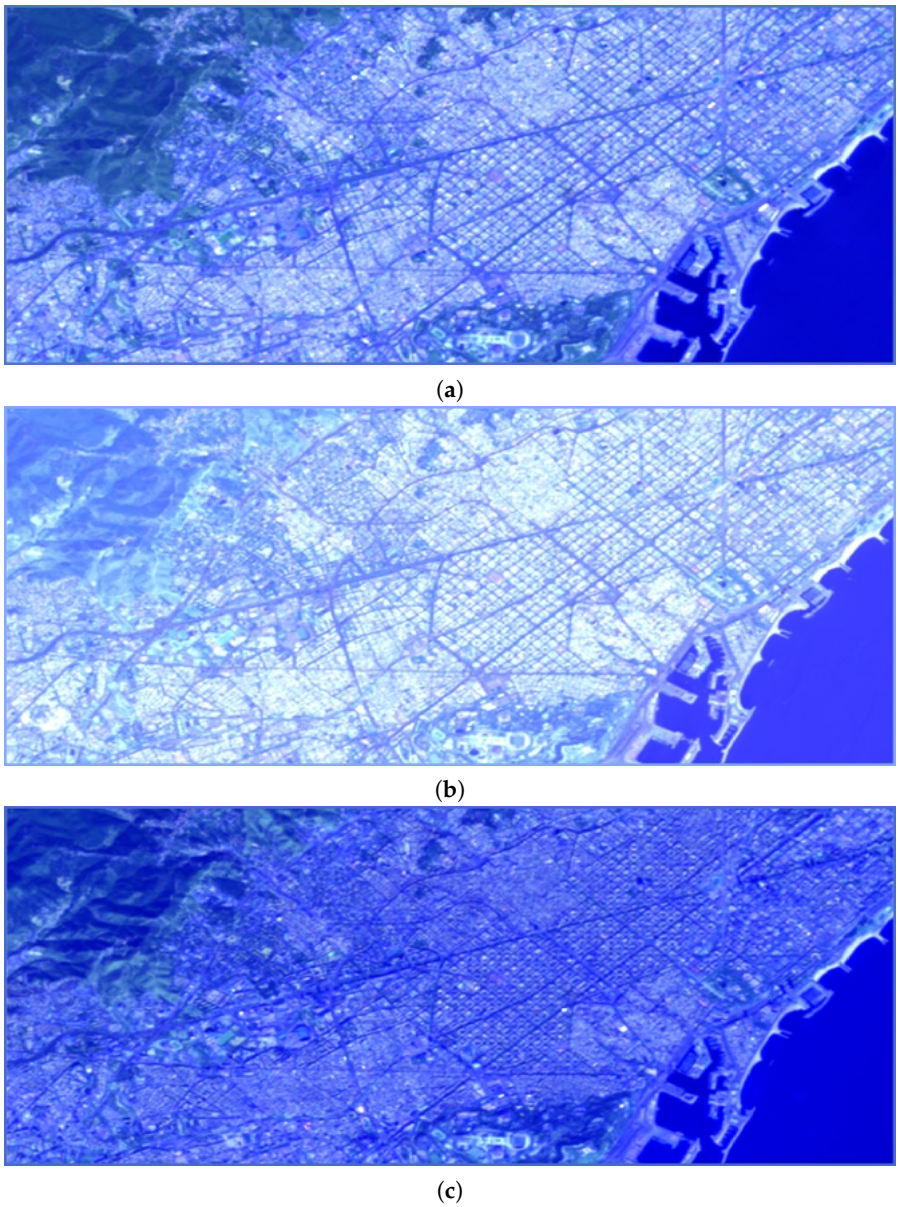

(**a**)

(**b**)

(**c**)

Figure 7. Some 90 km^2 portions of Barcelona Sentinel-2 TOA reflectance B12-B11-B1 false color compositions: (**a**), clear sky, 27 May 2020; (**b**), dust event, 21 July 2022; (**c**), biomass burning event, 25 October 2020.

The visual examination of the color compositions of spectral band data previously shown is further supported by an investigation of the reflectance spectra at the TOA. This analysis is relevant not only in relation to the whole observed area but also when concentrating on parts of the area that include water, if such parts are found within the study area. The graphical representations of TOA reflectance spectra, shown in Figures 11–13, where each point in the plot is the average of the corresponding band of one scene and is placed in the center wavelength of the band, highlight that the bands B2 to B4 and B11, B12 are those where the three cases of dust, smoke, and clear sky are easily distinguishable for each test image. It is important to note that the NIR bands are deliberately excluded from the analysis aimed at characterizing aerosols. The rationale behind this exclusion lies in the significant variation observed in TOA reflectances within these bands, a phenomenon largely attributable to seasonal fluctuations in the surface reflectance of vegetation.

(**a**)

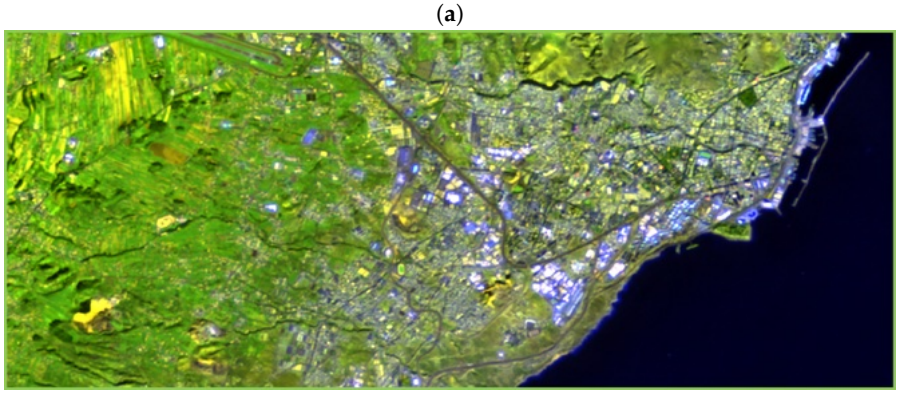

(**b**)

Figure 8. Some 90 km^2 portions of B4-B3-B2 (**a**) and B12-B11-B1 (**b**) color compositions of Sentinel-2 surface reflectance of the 1 January 2020 Tenerife reference acquisition. The yellow circle in (**a**) indicates the AERONET instrument position.

If the requirement of a temporally steady surface reflectance, or scene texture, motivates the exclusion of vegetation bands (B5, B6, B7, B8, B8a), an analogous requirement concerns water surfaces. Unless water is heavily polluted, water bodies do not have their own color, but reflect the color of the sky. This is clearly visible in Figures 12 and 13: the spectra measured on the land and on the sea are quite different. Unfortunately, the visible bands, where ocean color mostly appears, cannot be excluded from the analysis, because they are of crucial importance for discriminating biomass burning aerosols from clear sky. Therefore, we expect a loss of performance on water pixels. As a limit case, seasonal variations of the surface reflectance of vegetation moderately appear also in the green band (B3), or in the red band (B4) for maple forests. Upon inspection of the spectral plots in Figures 11–13, we notice that the blue band B2 is the least important among the visible bands for discriminating dust aerosols from smoke aerosols. If B2 were discarded in the analysis, color problems on the sea surface would be mitigated and the bands B3, B4, B11, and B12 would have the exact counterpart among the bands of the SLSTR instrument, mounted on the Sentinel-3 satellite constellation, providing daily observations at a 500 m scale. Also, Rayleigh scattering, decaying with the fourth power of the wavelength [36], would be abated if B2 were discarded.

In conclusion, the graphical representations shown in Figures 11–13 lay a solid foundation for the quantitative analysis of reflectance values at the TOA, specifically targeting the spectral bands B2 to B4 and B11, B12, for each image subjected to testing. This is the reason, for which five bands will be initially considered, instead of four or three. The choice of bands identifies their specificity in highlighting scattering phenomena involving particles of different dimensions, such as smoke and dust.

(**a**)

(**b**)

Figure 9. Some 90 km^2 portions of Tenerife Sentinel-2 TOA reflectance B4-B3-B2 color compositions: (**a**) clear sky, 14 February 2021; (**b**) extreme dust event, 30 January 2022.

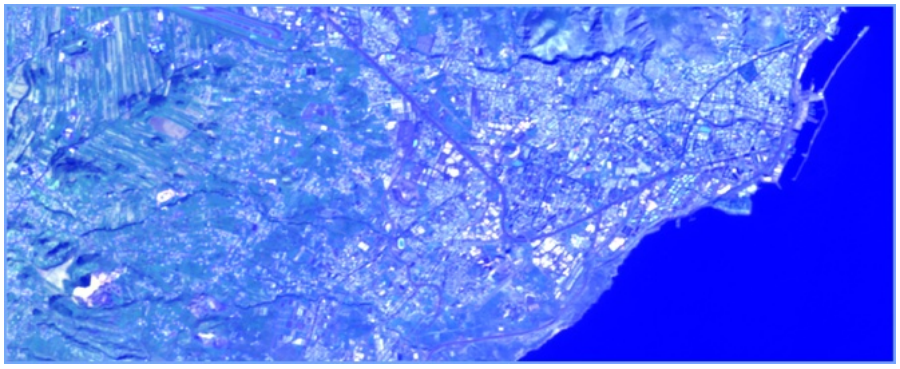

(**a**)

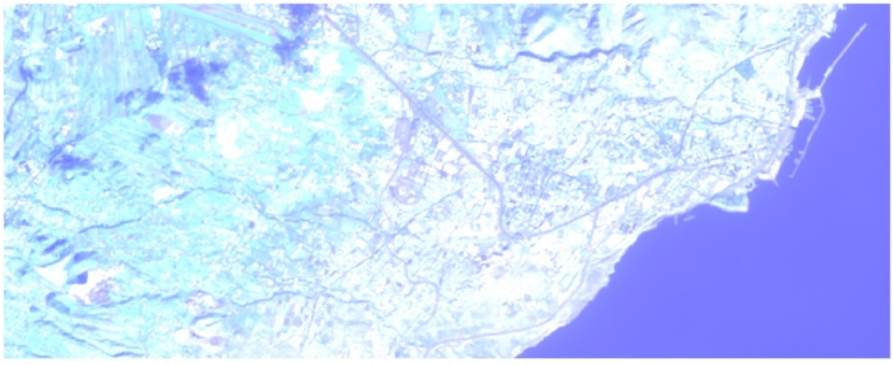

(**b**)

Figure 10. Some 90 km^2 portions of Tenerife Sentinel-2 TOA reflectance B12-B11-B1 color compositions: (**a**) clear sky, 14 February 2021; (**b**) extreme dust event, 30 January 2022.

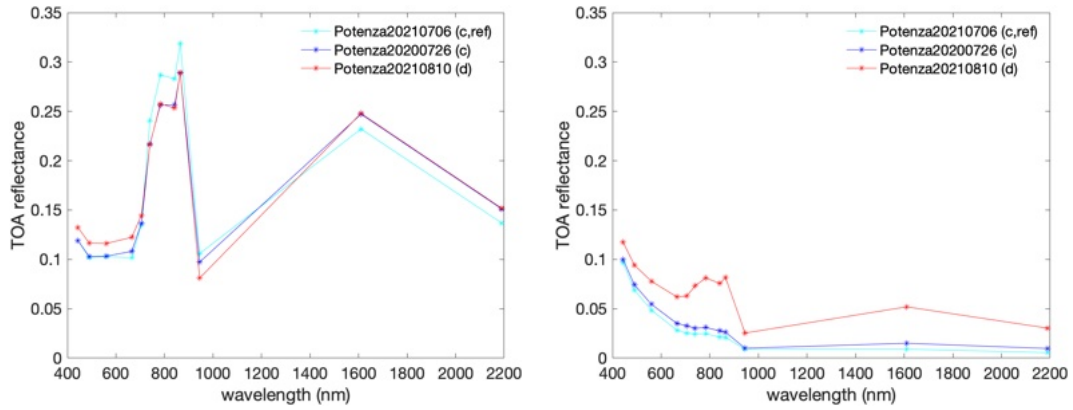

Figure 11. Potenza: TOA reflectance spectra (**a**) averaged over land and (**b**) over water pixels, for clear-sky reference (c, ref), almost clear sky (c), and dust event (d).

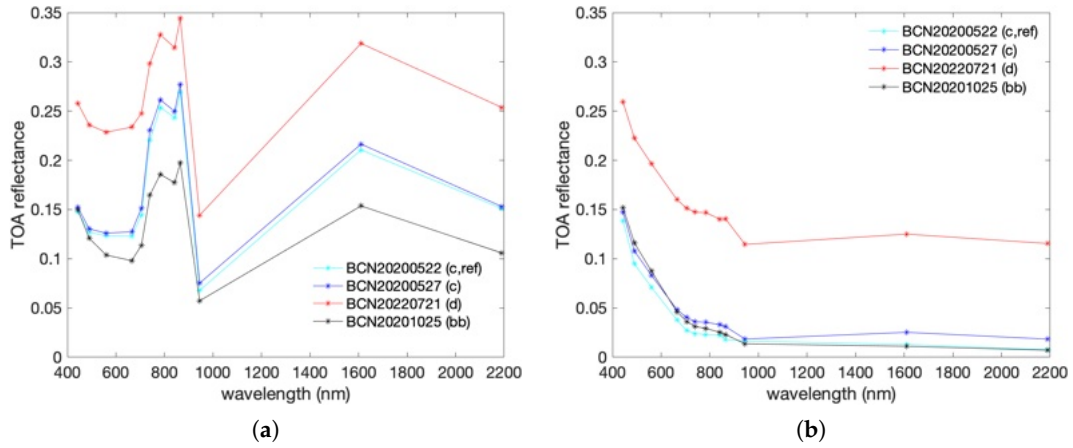

Figure 12. Barcelona: TOA reflectance spectra (**a**) averaged over land and (**b**) over water pixels, for clear-sky reference (c, ref), almost clear sky (c), dust (d) and biomass burning (bb) events.

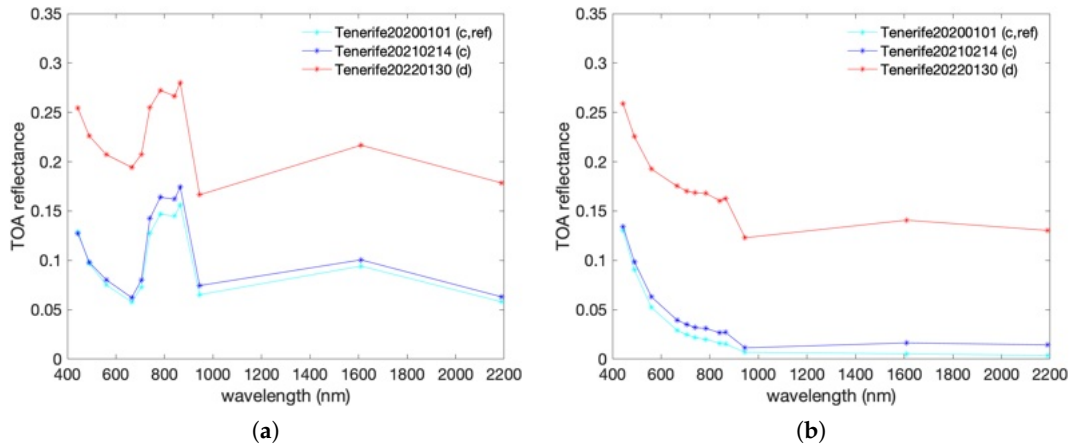

Figure 13. Tenerife: TOA reflectance spectra (**a**) averaged over land and (**b**) over water pixels, for clear-sky reference (c, ref), almost clear sky (c), and dust event (d).

2.4.2. A Spectral Index for Aerosol Characterization

Starting from the analysis previously described of the image color compositions of TOA reflectance bands and spatially averaged spectra in Figures 11–13, we developed the Dust/Biomass Burning (DBB) index of the pixel (i, j) to differentiate between smoke and dust aerosols in MS images of Sentinel-2 A/B. Such an index is (a) differential, because the

difference in responses on two dates, an aerosol event and clear sky, is considered as a sort of calibration that aligns these values; (b) normalized, because the index should be insensitive to the underlying scene, described by its surface reflectance; and (c) composite, because the specificity of different wavelengths, visible and SWIR, is averaged in a cumulative index:

$$\mathrm{DBB}(i,j) = \frac{1}{5}\sum_{k} \frac{\rho_k^{(\mathrm{TOA})}(i,j) - \overline{\rho}_k^{(\mathrm{TOA})}(i,j)}{\overline{\rho}_k(i,j)} \qquad k = 2,3,4,11,12 \tag{1}$$

where $\rho_k^{(\mathrm{TOA})}$ represents the TOA reflectance for the test image in the kth band, sourced from the L1C Sentinel-2 A/B product (refer to Figure 1), and $\overline{\rho}_k^{(\mathrm{TOA})}$ denotes the TOA reflectance from a reference capture at the same location, under clear atmospheric conditions, specifically where the combined aerosol coarse and fine mode AOD is below 0.07. The normalization term in Equation (1), $\overline{\rho}_k$, is the kth band of the L2A (surface reflectance) product of the reference image. The index in Equation (1) is computed at the pixel level to produce aerosol maps at either 10 m or 20 m spatial resolution, depending on whether the SWIR data are interpolated to 10 m or the R-G-B bands are downsampled to 20 m.

The spatial maps of the proposed DBB index provide a synoptic representation of the type and amount of aerosol, specifically (1) Saharan dust, which is highly reflective in the visible (2, 3, 4) and SWIR (11, 12) bands, thus increasing the DBB index (DBB > 0); conversely, (2) biomass burning aerosol (BBA) reduces TOA reflectance at the same wavelengths and consequently the DBB index (DBB < 0). For clear atmospheric conditions, typical values DBB ≈ 0 are observed.

To obtain a unique aerosol index, the proposed pixel index can be averaged across the scene, better on non-water pixels, because the normalizing term in Equation (1) may be unstable on water bodies, which exhibit unpredictable changes in time of their reflectance spectra (ocean color). Increased separability between dust and smoke aerosols can be achieved by averaging over areas in which water pixels have been discarded, whenever possible. Water pixels can be identified by thresholding the surface reflectance of B12 provided by the L2A product ($\rho_{12} < 1\%$).

3. Results

We now present the results obtained from the application of the Dust/Biomass Burning (DBB) index across various test locations. Table 2 presents DBB index values that were derived from spatial averaging of the DBB maps across different regions and dates. These values were calculated for water pixels and for land pixels. The DBB index serves as an indicator of aerosol type, with values greater than zero suggesting the presence of dust, and values less than zero indicating biomass burning. The coarse mode AOD retrieved by AERONET sunphotometer on a unique point of land is reported for comparisons.

For Tenerife, the index recorded on 1 January 2020 was identically zero for both water and the whole scene, being the reference clear-sky acquisition for this site. The value obtained from AERONET is nonzero because the definition of a clear sky is not based only on coarse-mode AOD. This was consistent on 14 February 2021, with a slight decrease in DBB (-0.01 on water, 0.05 on land), suggesting a negligible presence of smoke. AERONET AOD retrieves 0.1, because biomass burning affects only the AOD fine mode. However, on 30 January 2022, the DBB values increased significantly to 20.56 over water areas and 0.86 on land, clearly indicating a severe dust event (d), corroborated by the high value of AOD coarse mode (0.58). The abnormal value of the DBB on water indicates that the proposed index is not suitable for analyzing water areas because the surface reflectance during aerosol outbreaks may be much different from that on a clear day, by which the index is normalized.

In Potenza, the clear reference conditions, denoted as (c, ref), on 6 July 2021 show a DBB of 0 on both water and land. AERONET measured 0.1. On 26 July 2020 the value of DBB rose modestly to 0.01 on the tiny water patch of the scene and to 0.09 over land only, again suggesting a low presence of dust, otherwise measured by AERONET with a value

of coarse mode AOD 0.03. A more pronounced, but still limited, dust event is evident on 10 August 2021, with the index reaching values of 0.35 over water and 0.34 over land, while the AOD measure of AERONET is 0.12.

Barcelona's data show a reference value (c, ref) of 0 on 22 May 2020. The measure of AERONET on the clear reference day is 0.02. On 27 May 2020, the DBB index shows a slight increase of 0.11 in water and 0.09 in land. AERONET still finds 0.02. A substantial increase in the DBB to 4.24 on water and to 0.63 on land, on 21 July 2022, indicates a significant dust outbreak, confirmed by a value of 0.45 coarse mode AOD from AERONET. Eventually, on 25 October 2020, the DBB index drops below zero to an average value of −3.71 over water and −2.95 over land, suggesting a biomass burning event (bb). Coarse mode AOD value of 0.26 by AERONET does not follow the expected pattern, as the variable remains unaffected by biomass burning events.

Table 2. DBB values obtained by spatially averaging the DBB maps over water and land pixels. The coarse mode AOD measured by the AERONET instrument on land is reported for comparisons.

	DBB (Water)	DBB (Land)	AERONET
Tenerife 1 January 2020 (c, ref)	0	0	0.02
Tenerife 14 February 2021 (c)	−0.01	−0.05	0.01
Tenerife 30 January 20 (d)	20.56	0.86	0.58
Potenza 6 July 2021 (c, ref)	0	0	0.01
Potenza 26 July 2020 (c)	0.01	0.08	0.03
Potenza 10 August 2021 (d)	0.35	0.34	0.12
Barcelona 22 May 2020 (c, ref)	0	0	0.02
Barcelona 27 May 2020 (c)	0.11	0.09	0.02
Barcelona 21 July 2022 (d)	4.24	0.63	0.45
Barcelona 25 October 2020 (bb)	−2.95	−3.71	0.26

A synoptic view of the results in Table 2 is provided by the scatterplot between the values of DBB on land and AOD coarse mode from the AERONET sunphotometer, shown in Figure 14. The values of the three clear sky reference of each test site have been omitted, because the attribute of clear sky is related to factors other than coarse mode AOD, analogously to the presence of biomass burning aerosols, which would require fine mode AOD measurements. Thus, the values reported in Table 2 for the three reference cases and the biomass burning event in Barcelona have been discarded.

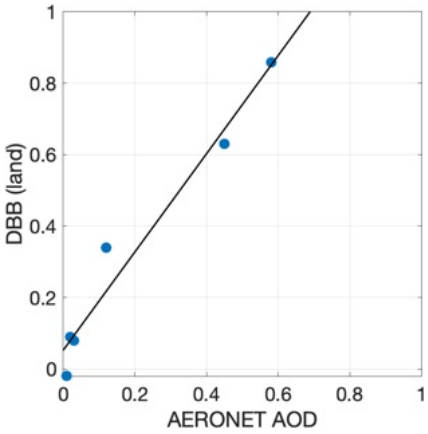

Figure 14. Scatterplot of average DBB values on land pixels versus AERONET coarse mode AOD measures (second and left column of Table 2). The three clear sky reference cases of DBB and the burning event in the last row have been discarded. The fit of the measures to the superimposed regression line is $R^2 = 96\%$.

Figure 14 witnesses an adequate match between DBB averaged on land and AERONET coarse mode AOD. The fit 96% is achieved by selecting only the pixel on the ground and

disregarding the biomass burning event in Barcelona. During dust outbreaks, DBB is reasonably non-negative and correlates with the AOD coarse mode. Why water pixels are unreliable and how the average values may differ from point measures on land will be explained by an inspection of the spatial maps of DBB in Figure 15.

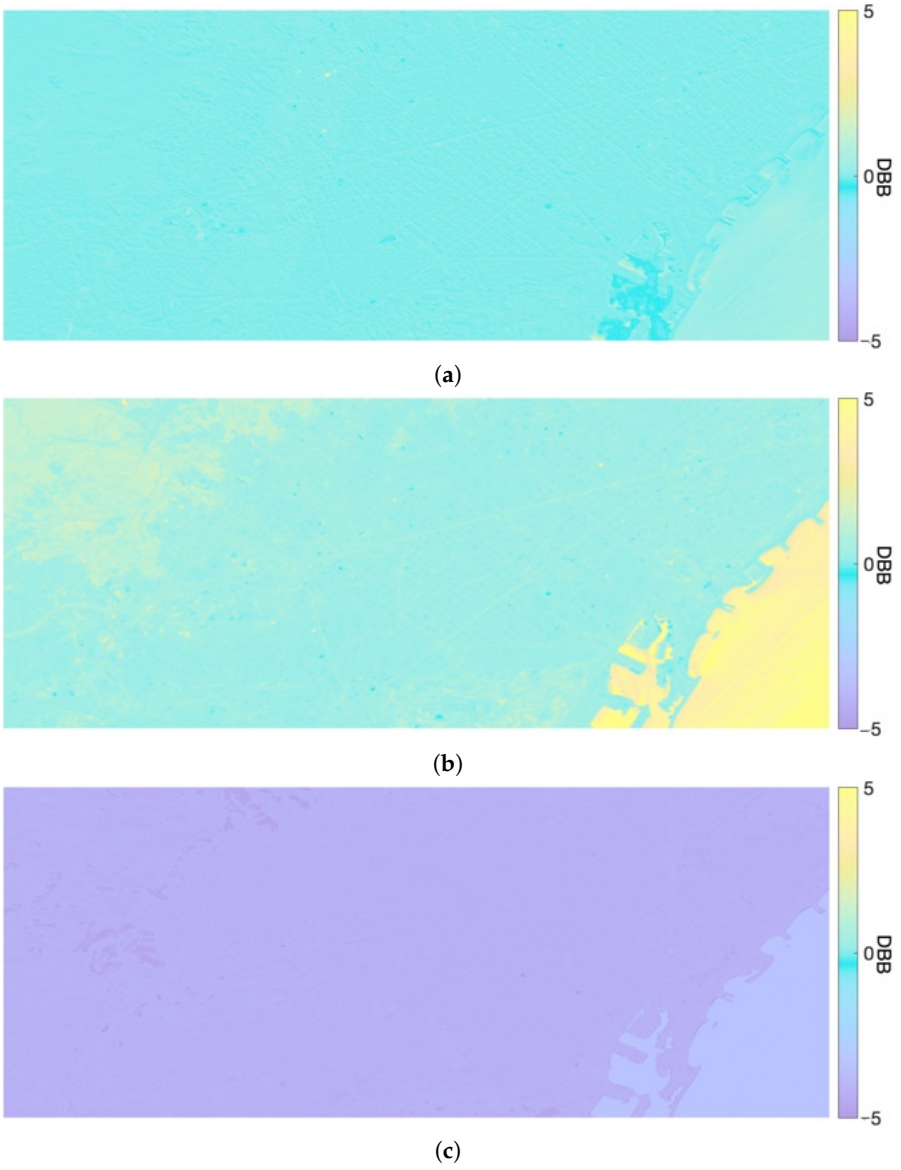

Figure 15. Some 90 km^2 portions of Barcelona Sentinel-2 DBB maps (**a**), clear sky, 27 May 2020; (**b**), dust event, 21 July 2022; (**c**), biomass burning event, 25 October 2020.

The Barcelona test site contains three cases: low aerosol loading, identified as dust by the index, consistent dust, and considerable burning biomass. The related maps of DBB are shown in the three panels of Figure 15. It is immediately apparent in all three maps that water pixels display a surprising level of aerosols, in contrast to the land, due to the significant and unpredictable alteration in the sea's surface reflectance on the event date compared to the reference clear sky date. In fact, the color of the sea is the reflection of atmosphere, which does not contain aerosols in the clear sky reference. The normalizing term in Equation (1), specifically introduced to remove the underlying texture from the aerosol map, should not change between the event and the reference dates. This is true only in an urban context, but definitely false over water and, in part on the vegetated region surrounding the outskirts, clearly visible in the map of Figure 15b. Thus, the index is more

accurate, where the surface reflectance remains unchanged over time. This is the reason why the texture of the city cannot be perceived on the maps of DBB.

4. Discussion

This study prototypes the measurement of aerosols at urban scale starting from routinely available satellite imagery. So far, spatial, spectral, and temporal constraints have drastically limited the choice of satellite instruments. The DBB composite index is tailored to Sentinel-2, due to its high-resolution MS imaging capabilities, which allow the differentiation of aerosol types based on their distinct spectral signatures. This method is not limited to Sentinel-2 data, but can be adapted for use with other sensors, provided that they offer similar MS imaging capabilities that allow the distinction between different types of aerosol. For example, the DBB index can be easily adjusted to work with SLSTR / Sentinel-3 imagery, whose spatial resolution (500 m), however, is unsuitable for street-level analysis. In this perspective, the two 100 m thermal infrared (TIR) bands of OLI would be invaluable for analyzing biomass burning events by detecting smoldering fires.

Being explicitly designed for urban environments, the method fails in measuring aerosols on water. The trivial reason is that the normalizing surface reflectance, necessary to remove the underlying texture of the scene from the map of aerosols, is highly unstable on water bodies, which do not have their own color, but reflect the color of the sky. This is the reason for which several aerosol products, e.g., MODIS, use different algorithms on land and water pixels. Another limitation concerns the presence of large vegetated regions in the scene, whose texture in the green band, crucial for the analysis of aerosols, may vary over time. The drawback of vegetation, however, is far less severe than that of water. Notwithstanding the problem of vegetation, the fit of DBB with AERONET data demonstrates that the accuracy of the proposed index seems to be reasonably high, at least for what concerns the detection of dusts. In the absence of a significant sample of test scenes with combustion aerosols, and related fine-mode AOD measures, the unique result on the detection of smoke should be considered preliminary and qualitative.

The proposed methodology based on the DBB index faces multiple challenges, mainly due to the constraints linked to the satellite's revisit time. The minimum 5-day revisit time of the Sentinel-2 twin satellites can potentially delay the detection and characterization of aerosol events, which can evolve or dissipate within this time frame, thereby affecting the timeliness and accuracy of collected data. The fusion of Sentinel-2 and Sentinel-3 data [43] would achieve an increase in the temporal resolution of the former. With proper fusion algorithms, including a correction for the haze term [44], the integrity of the spectral indices can be thoroughly preserved [45]. These limitations underscore the importance of integrating satellite data with ground-based observations and other data sources for comprehensive aerosol monitoring and characterization.

Future research will focus on addressing the previously raised issues and expanding this approach to geostationary satellites, which provide observations at much shorter intervals (every 10 min) rather than every five days, and feature a wide range of spectral bands. The third generation of MeteoSat, which features VNIR, SWIR, TIR, and the medium infrared (MIR) band, suitable for studying fires, could potentially provide more timely monitoring of aerosol events, at least on a scale of 1 Km. The tradeoff between time and spatial scale constraints can be relaxed by resorting to fusion of aerosol maps calculated separately from the data of each platform. By expanding the results to include data from geostationary satellites, researchers aim to improve the capabilities for continuous and real-time aerosol monitoring, thus improving understanding and management of their impacts on air quality, climate, and public health.

5. Conclusions

This paper presents an innovative approach to detecting and evaluating the presence of aerosol dust and biomass burning using multispectral (MS) images, particularly focusing on urban environments in the Mediterranean region. The authors introduce a dust/biomass

burning (DBB) composite index as a novel method to qualitatively assess the abundance and intensity of these aerosol types. The study uses data from the ESA Sentinel-2 twin satellite constellation, which offers high-resolution MS imaging capabilities every five days, alongside ground-based observations from the Aerosol Robotic Network (AERONET), to validate their findings. Key feature of the index is that it is insensitive to the underlying texture, which are particularly annoying and misleading in L2 products of high resolution MS satellite, e.g., the maps of AOD at different wavelengths of Sentinel-2 over urban areas.

Experiments have been conducted at three distinct locations, each chosen for their unique characteristics and relevance to the study of aerosols. These locations included areas near Potenza, Italy; Barcelona, Spain; and Tenerife, Canary Islands, Spain. By comparing the values of the DBB index derived from images taken during known aerosol events with those from clear-sky reference images, the study demonstrates the effectiveness of the index in distinguishing between dust outbreaks, biomass burning events, and clear atmospheric conditions. The correlation of DBB values with coarse mode AOD measures, carried out by instruments of the AERONET stations, attains 96%, notwithstanding that average DBB values on land are taken instead of pixel values at the instrument position.

The research findings indicate that the DBB index is a robust tool for differentiating between the two types of aerosol, with positive values indicating dust events and negative values indicating biomass burning. This differentiation is crucial to understanding the impact and variability over the years of these aerosols on air quality, climate, and human health. The results of the study, supported by visual inspections and spectral analyses, show a promising direction for future remote sensing research in aerosol characterization.

However, we acknowledge the existence of few areas where future enhancements can make the methodology even more robust. Presently, the index does not work properly on water pixels, typically sea/ocean. A small modification of the choice of bands that make up the composite index, or the definition of a different index for water pixels, as it happens with some aerosol products of MODIS, or a multiresolution approach using 500 m Sentinel-3 observations, could fix the inconvenience, since the spatial resolution of the aerosol map is not an asset on water bodies. Despite the five-day revisit period of Sentinel-2, which might not always capture rapidly evolving aerosol events, the data it provides are still invaluable. There are several opportunities to integrate it with other satellite- or ground-based observations for a more comprehensive view. The MS range of Sentinel-2 offers broad detection capabilities, and the absence of thermal infrared bands can inspire innovative methods to complement this with additional data sources. Lastly, leveraging a clear-sky baseline for comparison offers a solid foundation that, with precise calibrations, could yield even more accurate results in future studies.

In conclusion, this study provides significant information on aerosol remote sensing, offering a novel tool for the quantitative evaluation of biomass and dust combustion events. The ability of the DBB index, which relies on routinely available MS image data, to distinguish between different types of aerosol and to provide maps at a decametric scale is a valuable resource for researchers and policy makers alike, helping to develop strategies to mitigate the adverse effects of aerosol pollution on the environment and public health.

Author Contributions: Conceptualization and methodology: S.L., A.G. and L.A.; Validation and software: A.G. and A.A.; Data curation: A.G. and A.A.; Writing: S.L., L.A. and A.G. All authors have read and agreed to the published version of the manuscript.

Funding: This research received no external funding.

Institutional Review Board Statement: Not applicable.

Informed Consent Statement: Not applicable.

Data Availability Statement: Publicly available datasets were analyzed in the study. Image data can be found here: https://browser.dataspace.copernicus.eu (accessed on 30 April 2024). AERONET data are accessible from https://aeronet.gsfc.nasa.gov/ (accessed on 30 April 2024).

Acknowledgments: The authors would like to thank the NASA AERONET team for the AOD data.

Conflicts of Interest: The authors declare no conflicts of interest.

References

1. Baltensperger, U.; Prévôt, A. Chemical analysis of atmospheric aerosols. *Anal. Bioanal. Chem.* **2008**, *390*, 277–280. [CrossRef]
2. Milroy, C.; Martucci, G.; Lolli, S.; Loaec, S.; Sauvage, L.; Xueref-Remy, I.; Lavrič, J.V.; Ciais, P.; Feist, D.G.; Biavati, G.; et al. An assessment of pseudo-operational ground-based light detection and ranging sensors to determine the boundary-layer structure in the coastal atmosphere. *Adv. Meteorol.* **2012**, *2012*, 929080. [CrossRef]
3. Rosenfeld, D.; Lohmann, U.; Raga, G.; O'Dowd, C.; Kulmala, M.; Fuzzi, S.; Reissell, A.; Andreae, M. Flood or drought: How do aerosols affect precipitation? *Science* **2008**, *321*, 1309–1313. [CrossRef]
4. Kovadlo, P.; Shikhovtsev, A.; Lukin, V.; Kochugova, E. Solar activity variations inducing effects of light scattering and refraction in the Earth's atmosphere. *J. Atmos. Sol.-Terr. Phys.* **2018**, *179*, 468–471. [CrossRef]
5. Lolli, S. Is the air too polluted for outdoor activities? Check by using Your photovoltaic system as an air-quality monitoring device. *Sensors* **2021**, *21*, 6342. [CrossRef]
6. Campbell, J.R.; Ge, C.; Wang, J.; Welton, E.J.; Bucholtz, A.; Hyer, E.J.; Reid, E.A.; Chew, B.N.; Liew, S.C.; Salinas, S.V. Applying advanced ground-based remote sensing in the Southeast Asian Maritime Continent to characterize regional proficiencies in smoke transport modeling. *J. Appl. Meteorol. Climatol.* **2016**, *55*, 3–22. [CrossRef]
7. Landi, T.C.; Bonasoni, P.; Brunetti, M.; Campbell, J.R.; Marquis, J.W.; Di Girolamo, P.; Lolli, S. Aerosol direct radiative effects under cloud-free conditions over highly-polluted areas in Europe and Mediterranean: A ten-years analysis (2007–2016). *Remote Sens.* **2021**, *13*, 2933. [CrossRef]
8. Lewis, S.C.; King, A.D.; Perkins-Kirkpatrick, S.E.; Mitchell, D.M. Regional hotspots of temperature extremes under 1.5° C and 2° C of global mean warming. *Weather Clim. Extrem.* **2019**, *26*, 100233. [CrossRef]
9. Spiegl, T.; Langematz, U. Twenty-first-century climate change hot spots in the light of a weakening sun. *J. Clim.* **2020**, *33*, 3431–3447. [CrossRef]
10. Lolli, S.; Khor, W.Y.; Matjafri, M.Z.; Lim, H.S. Monsoon season quantitative assessment of biomass burning clear-sky aerosol radiative effect at surface by ground-based lidar observations in Pulau Pinang, Malaysia in 2014. *Remote Sens.* **2019**, *11*, 2660. [CrossRef]
11. Nakata, M.; Mukai, S.; Fujito, T. Direct detection of severe biomass burning aerosols from satellite data. *Atmosphere* **2022**, *13*, 1913. [CrossRef]
12. Knopp, L.; Wieland, M.; Rättich, M.; Martinis, S. A deep learning approach for burned area segmentation with Sentinel-2 data. *Remote Sens.* **2020**, *12*, 2422. [CrossRef]
13. Qin, K.; He, Q.; Zhang, Y.; Cohen, J.B.; Tiwari, P.; Lolli, S. Aloft transport of haze aerosols to Xuzhou, Eastern China: Optical properties, sources, type, and components. *Remote Sens.* **2022**, *14*, 1589. [CrossRef]
14. Lolli, S.; Sicard, M.; Amato, F.; Comeron, A.; Gíl-Diaz, C.; Landi, T.C.; Munoz-Porcar, C.; Oliveira, D.; Dios Otin, F.; Rocadenbosch, F.; et al. Climatological assessment of the vertically resolved optical and microphysical aerosol properties by lidar measurements, sun photometer, and in situ observations over 17 years at Universitat Politècnica de Catalunya (UPC) Barcelona. *Atmos. Chem. Phys.* **2023**, *23*, 12887–12906. [CrossRef]
15. Qu, J.J.; Hao, X.; Kafatos, M.; Wang, L. Asian dust storm monitoring combining Terra and Aqua MODIS SRB measurements. *IEEE Geosci. Remote Sens. Lett.* **2006**, *3*, 484–486. [CrossRef]
16. Osborne, M.; Malavelle, F.; Adam, M.; Buxmann, J.; Sugier, J.; Marenco, F.; Haywood, J. Saharan dust and biomass burning aerosols during ex-hurricane Ophelia: Observations from the new UK lidar and sun-photometer network. *Atmos. Chem. Phys.* **2019**, *19*, 3557–3578. [CrossRef]
17. Evgenieva, T.S.; Gurdev, L.; Toncheva, E.; Dreischuh, T. Aerosol types identification during different aerosol events over Sofia, Bulgaria, using sun-photometer and satellite data on the aerosol optical depth and Ångström exponent. *J. Phys. Conf. Ser.* **2022**, *2240*, 012027. [CrossRef]
18. Samulenkov, D.A.; Sapunov, M.V. The aerosol pollution of the atmosphere on the example of Lidar sensing data in St. Petersburg (Russia), Kuopio (Finland), Minsk (Belarus). *Geogr. Environ. Sustain.* **2023**, *16*, 156–163. [CrossRef]
19. Vivone, G.; Arienzo, A.; Bilal, M.; Garzelli, A.; Pappalardo, G.; Lolli, S. A dark target Kalman filter algorithm for aerosol property retrievals in urban environment using multispectral images. *Urban Clim.* **2022**, *43*, 101135. [CrossRef]
20. Ranjan, A.; Patra, A.K.; Gorai, A.K. A review on estimation of particulate matter from satellite-based aerosol optical depth: Data, methods, and challenges. *Asia-Pac. J. Atmos. Sci.* **2020**, *57*, 679–699. [CrossRef]
21. Ramachandran, S.; Kedia, S. Aerosol optical properties over South Asia from ground-based observations and remote Sensing: A review. *Climate* **2013**, *1*, 84–119. [CrossRef]
22. Samuel, C.; Kumar, R.P.; Gautam, S. Review of retrieval of aerosol optical depth to estimate particle concentration and its challenges based on spatiotemporal relationships by various spectroradiometer models. *Geol. J.* **2023**, *58*, 4403–4416. [CrossRef]
23. Wei, X.; Chang, N.; Bai, K.; Gao, W. Satellite remote sensing of aerosol optical depth: Advances, challenges, and perspectives. *Crit. Rev. Environ. Sci. Technol.* **2020**, *50*, 1640–1725. [CrossRef]
24. Li, Z.; Zhao, X.P.; Kahn, R.; Mishchenko, M.; Remer, L.; Lee, K.H.; Wang, M.; Laszlo, I.; Nakajima, T.; Maring, H. Uncertainties in satellite remote sensing of aerosols and impact on monitoring its long-term trend: A review and perspective. *Ann. Geophys.* **2009**, *27*, 2755–2770. [CrossRef]

25. Drusch, M.; Del Bello, U.; Carlier, S.; Colin, O.; Fernandez, V.; Gascon, F.; Hoersch, B.; Isola, C.; Laberinti, P.; Martimort, P.; et al. Sentinel-2: ESA's optical high-resolution mission for GMES operational services. *Remote Sens. Environ.* **2012**, *120*, 25–36. [CrossRef]
26. Sudmanns, M.; Tiede, D.; Augustin, H.; Lang, S. Assessing global Sentinel-2 coverage dynamics and data availability for operational Earth observation (EO) applications using the EO-Compass. *Int. J. Digital Earth* **2019**, *13*, 768–784. [CrossRef]
27. Alparone, L.; Arienzo, A.; Garzelli, A. Spatial resolution rnhancement of vegetation indexes via fusion of hyperspectral and multispectral satellite data. *Remote Sens.* **2024**, *16*, 875. [CrossRef]
28. Phiri, D.; Simwanda, M.; Salekin, S.; Nyirenda, V.R.; Murayama, Y.; Ranagalage, M. Sentinel-2 data for land cover/use mapping: A review. *Remote Sens.* **2020**, *12*, 2291. [CrossRef]
29. Alparone, L.; Garzelli, A.; Zoppetti, C. Fusion of VNIR optical and C-band polarimetric SAR satellite data for accurate detection of temporal changes in vegetated areas. *Remote Sens.* **2023**, *15*, 638. [CrossRef]
30. Yang, H.; Fang, Z.; Cao, Y.; Xie, C.; Zhou, T.; Wang, B.; Xing, K.; Lolli, S. Impacts of transboundary dust transport on aerosol pollution in the Western Yangtze River Delta Region, China: Insights gained from ground-based Lidar and satellite observations. *Earth Space Sci.* **2021**, *8*, e2020EA001533. [CrossRef]
31. Shendryk, Y.; Rist, Y.; Ticehurst, C.; Thorburn, P. Deep learning for multi-modal classification of cloud, shadow and land cover scenes in PlanetScope and Sentinel-2 imagery. *ISPRS J. Photogram. Remote Sens.* **2019**, *157*, 124–136. [CrossRef]
32. Ustin, S.L.; Middleton, E.M. Current and near-term advances in Earth observation for ecological applications. *Ecol. Process.* **2021**, *10*, 1. [CrossRef]
33. Aiazzi, B.; Alparone, L.; Barducci, A.; Baronti, S.; Pippi, I. Estimating noise and information of multispectral imagery. *Opt. Eng.* **2002**, *41*, 656–668. [CrossRef]
34. Aiazzi, B.; Alparone, L.; Baronti, S.; Garzelli, A.; Selva, M. Advantages of Laplacian pyramids over "à trous" wavelet transforms for pansharpening of multispectral images. In *Image and Signal Processing for Remote Sensing XVIII*; Bruzzone, L., Ed.; International Society for Optics and Photonics, SPIE: Bellingham, WA, USA, 2012; Volume 8537, pp. 12–21. [CrossRef]
35. Main-Knorn, M.; Pflug, B.; Louis, J.; Debaecker, V.; Müller-Wilm, U.; Gascon, F. Sen2Cor for Sentinel-2. In *Image and Signal Processing for Remote Sensing XXIII*; Bruzzone, L., Ed.; International Society for Optics and Photonics, SPIE: Bellingham, WA, USA, 2017; Volume 10427, p. 1042704. [CrossRef]
36. Pacifici, F.; Longbotham, N.; Emery, W.J. The importance of physical quantities for the analysis of multitemporal and multiangular optical very high spatial resolution images. *IEEE Trans. Geosci. Remote Sens.* **2014**, *52*, 6241–6256. [CrossRef]
37. Arienzo, A.; Aiazzi, B.; Alparone, L.; Garzelli, A. Reproducibility of pansharpening methods and quality indexes versus data formats. *Remote Sens.* **2021**, *13*, 4399. [CrossRef]
38. Holben, B.N.; Eck, T.F.; Slutsker, I.; Tanre, D.; Buis, J.P.; Setzer, A.; Vermote, E.; Reagan, J.A.; Kaufman, Y.J.; Nakajima, T.; et al. AERONET—A federated instrument network and data archive for aerosol characterization. *Remote Sens. Environ.* **1998**, *66*, 1–16. [CrossRef]
39. O'Neill, N.; Eck, T.; Smirnov, A.; Holben, B.; Thulasiraman, S. Spectral discrimination of coarse and fine mode optical depth. *J. Geophys. Res. Atmos.* **2003**, *108*, 1–15. [CrossRef]
40. Arola, A.; Eck, T.; Kokkola, H.; Pitkänen, M.; Romakkaniemi, S. Assessment of cloud related fine mode AOD enhancements based on AERONET SDA product. *Atmos. Chem. Phys.* **2014**, *17*, 5991–6001. [CrossRef]
41. Torres, B.; Dubovik, O.; Fuertes, D.; Schuster, G.; Cachorro, V.; Lapyonok, T.; Goloub, P.; Blarel, L.; Barreto, A.; Mallet, M.; et al. Advanced characterisation of aerosol size properties from measurements of spectral optical depth using the GRASP algorithm. *Atmos. Measur. Tech.* **2016**, *10*, 3743–3781. [CrossRef]
42. Giles, D.M.; Sinyuk, A.; Sorokin, M.G.; Schafer, J.S.; Smirnov, A.; Slutsker, I.; Eck, T.F.; Holben, B.N.; Lewis, J.R.; Campbell, J.R.; et al. Advancements in the Aerosol Robotic Network (AERONET) Version 3 database–automated near-real-time quality control algorithm with improved cloud screening for Sun photometer aerosol optical depth (AOD) measurements. *Atmos. Measur. Tech.* **2019**, *12*, 169–209. [CrossRef]
43. Wang, Q.; Atkinson, P.M. Spatio-temporal fusion for daily Sentinel-2 images. *Remote Sens. Environ.* **2018**, *204*, 31–42. [CrossRef]
44. Vivone, G.; Alparone, L.; Garzelli, A.; Lolli, S. Fast reproducible pansharpening based on instrument and acquisition modeling: AWLP revisited. *Remote Sens.* **2019**, *11*, 2315. [CrossRef]
45. Garzelli, A.; Aiazzi, B.; Alparone, L.; Lolli, S.; Vivone, G. Multispectral pansharpening with radiative transfer-based detail-injection modeling for preserving changes in vegetation cover. *Remote Sens.* **2018**, *10*, 1308. [CrossRef]